Modeling of particulate coagulation in low pressure plasmas

U. Kortshagen and U. Bhandarkar
Department of Mechanical Engineering, University of Minnesota, 111 Church Street Southeast, Minneapolis, Minnesota 55455
(Received 22 September 1998)

In this paper we study the growth of nanometer particles in low pressure plasmas due to coagulation. We describe results of a model which involves the self-consistent determination of plasma properties, the description of particle charging, as well as the description of the particle size distribution via solution of the general dynamic equation for an aerosol. Our results show that particle coagulation in the low pressure plasma is enhanced compared to coagulation in neutral aerosols due to the attraction of oppositely charged particles. The temporal behavior of the coagulation follows the same laws as coagulation of neutral particles as long as the density of nanometer particles is larger than the positive ion density in the plasma. The positive ion density can be considered as the critical density for coagulation to occur. We also show that the details of the particle charging mechanism are only of minor importance for the coagulation dynamics but of great importance for the accurate prediction of plasma parameters. [S1063-651X(99)01407-5]

PACS number(s): 52.90.+z, 52.80.Pi

I. INTRODUCTION

The generation of particulates ranging in size from a subnanometer scale up to hundreds of micrometers has been observed in practically all processing plasmas used for semiconductor manufacturing [1–3]. Particle contaminations are considered one of the major causes for device yield loss. The current National Technology Roadmap for Semiconductors (NTRS) projects that the characteristic feature size will shrink from 0.25 μm in 1997 to 0.05 μm by 2012. It is believed that particles with one-third the feature size represent potential ''killer particles'' if they deposit on a wafer during processing. Thus, over the next fifteen years the killer particle diameter will shrink from currently 80 nm to less than 20 nm. Consequently, the understanding of contaminant particle growth is identified as one of the most urgent problems for contamination-free semiconductor manufacturing.

Killer particles in processing plasmas originate either from gas phase nucleation or from fracture of films deposited on the walls or the wafer [4]. Gas phase nucleation was for a long time believed to be important mainly in plasma-enhanced chemical-vapor deposition (PECVD) systems [5,6]. However, the structure of submicron particles recently observed in an SF_6 etching plasma [7] suggests that gas phase nucleation may also play an important role in etch plasmas. Nanometric particles can nucleate within fractions of a second in PECVD systems. Since such small particles are at the detection limit of current *insitu* particle diagnostics techniques, many plasmas which are believed to be particle-free might actually be strongly contaminated with nanoparticles.

While research on particles in processing plasmas initially focussed on the control or avoidance of ''killer particulates,'' recently the benefits of the deliberate, controlled generation of nanoparticles in plasmas were pointed out. For instance, SiC particles were prepared and trapped in an rf glow discharge and then coated with palladium in the same reactor for applications as microcatalysts [8,9]. Another example of possible applications of nanoparticles generated in low pressure rf plasmas is the preparation of nanocrystalline films. In experiments on *a*-Si:H thin film deposition it was shown that under certain conditions nanoparticles with a diameter of a few nanometer escape from the plasma and are incorporated into films [10,11]. These nanocrystalline films hold promise to yield superior performance in solar cells compared to amorphous silicon films [12,13].

For both these aspects, the avoidance of ''bad'' particles as well as the innovative use of ''good'' particles, a thorough understanding of the growth mechanisms of nanoparticles in plasmas and of their growth kinetics is required. Experiments conducted in SiH_4 plasmas have led to a three phase picture of the particle growth in many PECVD systems [5,6]: During the first phase of about 100 ms initial spherical crystallites nucleate within the plasma and grow to a diameter of about 2 nm which corresponds to on the order of 1000 atoms per particle. Once the particles have reached this size, a phase of rapid particle growth by coagulation of the primary particles sets in. The coagulation phase prevails for about 5 sec and the particles grow to a size of about 50–60 nm in diameter. When the particles have reached this size, the coagulation process stops and particles continue to grow by molecular sticking of SiH_x clusters (third phase). During the entire process the particle size distribution remains rather monodisperse. Moreover, dramatic changes of the plasma properties during coagulation have been observed.

In the present paper we will focus on the second phase of the growth of nanoparticles due to coagulation. The coagulation phase has been studied extensively by numerous groups [5,6,14,15]. Some distinct physical features have been observed during the coagulation process.

(i) The coagulation phenomenon only occurs when the initial particle concentration reaches a critical value of about $10^{10}-10^{11}$ cm^{-3} [16].

(ii) A drastic increase of the electron temperature from about 2 eV before coagulation to about 8 eV after coagulation has been observed. This phenomenon is referred to as the α-γ' transition in the literature [5,17].

Some theoretical attempts have been made to explain these experimental results. Courteille *et al.* [15] interpret their experimental results on particle coagulation in terms of a Brownian free molecule coagulation (BFMC) of neutral

particles. Reasonable agreement between particle densities calculated with this model and measured densities is found. This, however, seems slightly surprising since the authors also demonstrate that the average charge of particles a few nanometers in diameter is much less than one elementary charge. Particles with such small a charge should be subject to strong statistical charge fluctuations [18,19]. As pointed out by Matsoukas *et al.* [20] this statistical charge fluctuation should lead to an increase in the coagulation rate compared to neutral coagulation. Watanabe *et al.* [21] arrive at the same conclusion that the coagulation rate in their experiment is actually faster than the thermal coagulation rate, most likely due to attraction of particles with unlike charges.

The charging of particles during the coagulation process was taken into account by Schweigert and Schweigert [22]. The authors consider charging of particles due to collection of electrons and ions. They arrive at the conclusion that most of the particles are actually negatively charged. However, a comparison of their results with the experimental results of Bouchoule and Boufendi [5,6] shows that the coagulation rates obtained from their model are by an order of magnitude smaller than those observed in experiments. Kim and Ikegawa [23] use a similar approach but also find extremely small coagulation rates.

In summary, in spite of intensive studies over the past years the picture of the coagulation mechanism of particles in low pressure plasmas is still rather inconsistent. Part of this problem may be based on the fact that in none of the previous studies the plasma parameters are actually self-consistently determined. Schweigert and Schweigert assume a constant electron density during coagulation, Courteille *et al.* assume constant electron temperature and electron and ion density. In experiments, however, these parameters have been found to change considerably. Since the ratio of electron to ion density as well as the electron temperature significantly affect the particle charge distribution, it seems to be necessary to take into account the temporal evolution of these parameters during the coagulation process.

In this paper we discuss a model which addresses the coagulation of nanometer particles using self-consistent plasma parameters. We also study the influence of previously neglected physical processes which may affect the particle charge. These processes are photodetachment of electrons from particles due to UV photons, secondary electron emission due to energetic electrons generated in the sheaths of capacitive rf discharges, and detachment due to quenching of excited atoms at the particle surface. We will use this model to comment on the aspects of the ''critical density'' and the α-γ' transition.

The paper is organized as follows. In Sec. II we describe the model developed. In Sec. III we present results and discussion. In Sec. IV we summarize the main results and discuss their potential importance for the control of particle coagulation in plasmas.

II. PARTICLE COAGULATION MODEL

Our particle coagulation-plasma model consists of three modules which are coupled in a self-consistent, iterative numerical scheme. These modules deal with the charging of particles, their coagulation, and with the self-consistent determination of plasma properties.

A. Particle charging

Following Schweigert and Schweigert [22] and Matsoukas [19,20], the electron and ion currents collected by a particle in the nanometer regime can be described by the orbital-motion-limited (OML) probe theory. A particle with radius R_p which carries a charge $Z_k = ke$ (with e the elementary charge and k an integer) is charged to a surface potential of $\Phi_k = Z_k/4\pi\epsilon_0 R_p$, with ϵ_0 the vacuum dielectric constant. Using OML theory [24], expressions for the frequency with which a particle with charge Z_k is hit by electrons and ions, respectively, can be derived [22,19]:

$$\nu_{e,i}^k = n_{e,i} S v_{e,i} \exp\left(-\frac{q_{e,i}\Phi_k}{k_B T_{e,i}}\right), \quad q_{e,i}\Phi_k \geq 0$$

$$= n_{e,i} S v_{e,i}\left(1 - \frac{q_{e,i}\Phi_k}{k_B T_{e,i}}\right), \quad q_{e,i}\Phi_k < 0. \tag{1}$$

$S = 4\pi R_p^2$ is the particle surface area, $v_{e,i} = (k_B T_{e,i}/2\pi m_{e,i})^{1/2}$, $n_{e,i}$ stands for the electron and ion densities, $m_{e,i}$ and $T_{e,i}$ are the mass and temperature of electrons and ions, respectively, and $q_{e,i} = \mp e$ is the respective charge. k_B is the Boltzmann constant.

It should be stressed that if only electron and ion capture are considered, the huge difference in electron and ion mass and temperature leads to strongly negative particles [22], unless it is balanced by the ion density being much larger than the electron density. In addition to charging due to electron and ion collection we also consider the interaction of UV photons with charged particles. We refer to this process as UV photodetachment (UVPD). Many of the coagulation experiments have been conducted in SiH_4 highly diluted in Ar or He. It is well known that in pure rare gas discharges up to about 50% of the electrical power can be transfered into UV resonance radiation. Since resonance radiation is strongly trapped in the plasma, the UV photon flux in the plasma can be orders of magnitude higher than the photon flux emerging from the discharge, similar to an optical resonator with a high quality factor. Typical UV resonance radiation in the plasma has energies between 10 and 20 eV. The binding energy of an electron attached to a singly negatively charged Si:H nanoparticle is between the electron affinity of bulk silicon of 4.07 eV and that of a Si^- negative ion of 1.2 eV. Recent studies have demonstrated that even for large silicon clusters the electron affinity is significantly reduced compared to the bulk material affinity [25–29]. Stoffels *et al.* speculate that the electron affinity of Si:H may be even as low as 1.5 eV. However, while UVPD is a process which is definitely energetically possible, little is known about the efficiency of photodetachment from nanoparticles. The ''straightforward estimate'' of assuming that nanoparticles absorb radiation with the absorption cross section in the Rayleigh approximation and emit photons with a quantum yield of the bulk material is highly questionable. Indeed, it has been proven highly erroneous for nanoparticles from several metals in numerous studies of Schmidt-Ott, Siegmann, and co-workers [30–35]. Abnormally high quantum yields of up

to one electron per incident photon from uncharged nanoparticles of Ni, Pd, Cu, Ag, and Au have been observed. These quantum yields are up to two orders of magnitude larger than those of the respective bulk materials [30,33,35]. The increased photon yield of nanoparticles can at least in part be explained by curvature effects of the surface [36,37]. Due to the lack of better information for Si:H particles we assume similar quantum yields Q as for metal particles between 0.25 and 1.0 electron per incident photon.

In order to determine the photon flux which hits the particle surface, we assume that UV resonance radiation is emitted from the Ar background gas. Ar has two resonance radiative levels ($^3P_1$ and $^1P_1$) with transition probabilities of $A_1=1.19\times10^8$ s^{-1} and $A_2=5.8\times10^8$ s^{-1}. Since resonance radiation can be absorbed by atoms in the ground state one has to consider the probability $\mathcal{T}$ that a photon emitted from an excited atom will reach a particle at a distance ρ. Assuming that both Doppler and pressure broadening are present, the line profile of emission and absorption have to be described by a Voigt profile $P(\nu)$, and the probability is given by [38]

$$\mathcal{T}(\rho)=\int_{-\infty}^{+\infty}P(\nu)\exp[-\kappa P(\nu)\rho]d\nu, \tag{2}$$

with ν the photon frequency, κ the absorption coefficient [38], and $\int_{-\infty}^{+\infty}P(\nu)=1$. In spherical coordinates with the particle at the origin, a volume element at a distance ρ from the particle contributes the differential photon flux:

$$d\Gamma_{1,2}=n_{1,2}A_{1,2}\frac{d\omega}{4\pi}\mathcal{T}_{1,2}(\rho)\rho^2\sin\Theta d\Theta d\phi d\rho, \tag{3}$$

with $d\omega=\pi R_p^2/\rho^2$ the solid angle under which the particle is seen from the volume element, and $n_{1,2}$ the population density of the $^3P_1$ and $^1P_1$ level, respectively. Integrating over volume yields the charging frequency by resonance UV photodetachment:

$$\nu_{\gamma,1,2}=Q\pi R_p^2 n_{1,2}A_{1,2}\int_0^{R_0}\mathcal{T}_{1,2}(\rho)d\rho. \tag{4}$$

The population densities $n_{1,2}$ are determined self-consistently by the plasma model along with the electron temperature and density, and the ion density. R_0 is a typical discharge dimension.

Electrons may also be detached from particles due to collisions with excited atoms. The charging frequency due to this quenching process is given by

$$\nu_{qu}=(n_1+n_2)\sqrt{k_BT/m_a}\pi R_p^2, \tag{5}$$

with T the gas temperature and m_a the atomic mass.

Lastly, we also consider secondary electron emission (SEE) due to energetic electrons generated in the rf sheaths of the capacitive rf discharge. These electrons are released by ions impinging on the electrodes and they are accelerated in the high fields of the rf sheath. We roughly assume that these electrons have on average a kinetic energy of 1/2 the maximum sheath voltage $V_{\rm sh}$. The density of energetic electrons in the discharge region can be estimated from the balance of energetic electrons entering the discharge through the sheaths and the energy relaxation rate of energetic electrons due to inelastic collisions with atoms and collisions with particles:

$$n_{h,e}=\frac{\Gamma_{h,e}A_s}{V\tau_{h,e}}. \tag{6}$$

$\Gamma_{h,e}$ is the flux of energetic electrons which is given by

$$\Gamma_{h,e}=\gamma_i\Gamma_i=\gamma_i\frac{n_iD_a}{l} \tag{7}$$

with γ_i the secondary electron coefficient for electron release from the electrodes due to ions, metastables, and photons [39], Γ_i the ion flux, n_i the ion density, $D_a=k_BT_e/m_i\nu_{cx}$ the well-known ambipolar diffusion coefficient, and l a typical diffusion length. A_s and V in Eq. (6) denote the surface area of the electrodes and the discharge volume, respectively. The lifetime of energetic electrons with respect to energy relaxation due to collisions is given by

$$\frac{1}{\tau_{h,e}}=n_p(\pi R_p^2)v_{h,e}+N_0\left(\frac{2u_i}{V_{\rm sh}}Q_{i,h}+\frac{2u_{\rm ex}}{V_{\rm sh}}Q_{{\rm ex},h}\right)v_{h,e}, \tag{8}$$

with n_p the particle density, N_0 the gas atom density, $Q_{i,h}$ and $Q_{{\rm ex},h}$ the cross sections for ionization and total excitation at 1/2 $V_{\rm sh}$, u_i and $u_{\rm ex}$ the threshold energies for ionization and excitation, and $v_{h,e}=\sqrt{eV_{\rm sh}/m_e}$. The charging frequency due to secondary electron emission caused by impact of energetic electrons is given by

$$\nu_{se}=n_{h,e}(\pi R_p^2)v_{h,e}(\delta-1), \tag{9}$$

where δ is the coefficient for secondary electron release from the particle. As pointed out recently by Perrin and Hollenstein, this coefficient can become as large as about 5 depending on the energy of energetic electrons and on the size of the Si:H particles [40]. This value is much larger than the value for bulk Si material of $\delta\approx1.5$ for similar reasons as discussed above with regard to UV photodetachment.

The charge distribution of particles of a given radius R_p is described by the fraction of particles F_k carrying a charge ke. It is normalized by $\Sigma_kF_k=1$. We use the rough approximation that the charging frequencies due to photodetachment, quenching of excited states, and due to secondary electron release are independent of the charging state of the particle. The rate equation for a charge state k can then be written as

$$\frac{dF_k}{dt}=\nu_e^{k+1}F_{k+1}-\nu_e^kF_k-(\nu_i^k+\nu_{\gamma,1}+\nu_{\gamma,2}+\nu_{qu}+\nu_{se})F_k+(\nu_i^{k-1}+\nu_{\gamma,1}+\nu_{\gamma,2}+\nu_{qu}+\nu_{se})F_{k-1}. \tag{10}$$

Under most circumstances, the charging of particles is much faster than coagulation so the charge distribution can be considered in steady state [22], i.e., $dF_k/dt\approx0$. This assumption enables the use of recursive relations for the charge distribution

$$F_{k+1}=\frac{\nu_i^k+\nu_{\gamma,1}+\nu_{\gamma,2}+\nu_{qu}+\nu_{se}}{\nu_e^{k+1}}F_k. \tag{11}$$

Starting with $F_0=1$ and subsequent normalization enables efficient calculation of the charge distribution for positive and negative charges.

B. Particle coagulation

Coagulation of particles has been studied for decades in the aerosol literature. A wide variety of techniques is available to model coagulation [41]. However, only a few studies have considered coagulation of charged particles [42–46] and these studies usually do not apply to conditions in low pressure processing plasmas.

The scenario of coagulation of particles in a low pressure plasma is identical to that of coagulation in a bipolar aerosol [43,46]. In general, the temporal evolution of the charge distribution and of the particle size distribution have to be considered simultaneously, leading to rather elaborate numerical schemes [43,46]. However, the fact that the time for particle charging is typically much shorter than the typical coagulation time [22] allows us to separate the problems of charging and coagulation from each other. Thus, we treat the coagulation process using the equations for neutral aerosols and we account for particle charging by using modified coagulation rates. However, we note that the results of our model may be inaccurate due to this separation for times less than about 10^{-3} s.

The particle distribution function is usually considered in terms of the particle volume v. If $n(v)$ denotes the particle number density in a volume range $[v,v+dv]$, the temporal evolution of $n(v)$ is described by the general dynamic equation (GDE) for an aerosol [47]

$$\frac{\partial n(v)}{\partial t}=\frac{1}{2}\int_0^v \beta(v',v-v')n(v')n(v-v')\,dv' - \int_0^\infty \beta(v,v')n(v)n(v')\,dv'. \tag{12}$$

The first term on the right hand side accounts for the gain of particles within the volume range $[v,v+dv]$ due to coagulation of smaller particles. The second term describes the loss of particles from the same volume element due to coagulation with particles of any volume. $\beta(v,v')$ is the frequency for coagulation between two particles with a volume v and v'. Assuming free molecular regime, β is given by [48]

$$\beta(v,v')=\alpha(v,v')\left(\frac{3}{4\pi}\right)^{1/6}\left(\frac{6k_BT}{\rho_p}\right)^{1/2}\left(\frac{1}{v}+\frac{1}{v'}\right)^{1/2} \times(v^{1/3}+v'^{1/3})^2, \tag{13}$$

where v and v' are the volumes of the particles interacting, ρ_p is the density of the particles, and T is the temperature of the particles. $\alpha(v,v')$ is a coefficient which describes that the effective cross section for coagulation depends on the charge of both particles. Assuming the cross section given by the OML theory yields

$$\alpha(v,v')=\sum_{k=-\infty}^{\infty}\sum_{k'=-\infty}^{\infty}F_k(v)F_{k'}(v')\mathcal{Q}(k,k',v,v') \tag{14}$$

with

$$\mathcal{Q}(k,k',v,v')=\exp\left(-\frac{kk'e^2}{4\pi\epsilon_0R_sk_BT}\right),\quad kk'>0 =1-\frac{kk'e^2}{4\pi\epsilon_0R_sk_BT},\quad kk'\leq 0, \tag{15}$$

and $R_s=(3/4\pi)^{1/3}(v^{1/3}+v'^{1/3})$.

Instead of solving the GDE (12) directly, which would imply solving a complicated integral equation we use a sectional model [49,50], a method well known in the aerosol literature. Briefly, the domain of volume considered is divided on a logarithmic scale into equal sections. Instead of the particle volume distribution $n(v)$ the general aerosol property $q(v)=\gamma v^m n(v)$ is considered, which is assumed to be constant within each section. By using the appropriate coefficient γ and exponent m, the same method can be used to describe the number density ($\gamma=1$, $m=0$), the volume ($\gamma=1$, $m=1$), and the surface area ($\gamma=\pi^{1/3}6^{2/3}$, $m=2/3$). By integrating $q(v)$ over each section, a set of rate equations for the integrated aerosol property is derived. The coagulation frequency β appears in integral coefficients, which have to be evaluated only once at the beginning of the calculation if $\alpha(v,v')$ is factored out of the integral. Only the coefficients $\alpha(v,v')$ have to be updated during the coagulation process to account for changes in the plasma conditions and of the particle charge distribution. The charge distribution during the coagulation process has to be determined for particles in each section, since the particle charge distribution depends on the particle radius.

In our case, we consider particles between 1 and 100 nm radius. We thus have to cover six decades for the particle volume. We divide the volume range into 180 sections. The volume at the right boundary of each section is by a factor 1.08 larger than that at the left boundary. The set of rate equations is propagated in time using an explicit scheme. A particular advantage of the formulation of the problem in volume is that the code is inherently volume conserving.

C. Plasma properties

For a given particle radius R_p, the particle charge depends on the electron density n_e, the ion density n_i, the electron temperature T_e, and, if photodetachment, quenching, and secondary electron emission turn out to be important, on the number densities of excited Ar atoms n_1 and n_2, and the density of energetic electrons $n_{e,h}$. The ion temperature can be assumed to be close to room temperature, i.e., $T_i\approx 300$ K. The density of energetic electrons $n_{e,h}$ is determined by Eq. (6). In order to self-consistently determine the remaining five unknown quantities, we use a simple global plasma model.

The first equation used is the ion balance equation accounting for ion loss to the electrodes and to the particles, as well as ion production due to ionization by low energetic

plasma electrons with temperature T_e and energetic electrons coming for the sheaths

$$n_i \frac{D_a}{l} A_s + n_i \nu_{ip} V = [n_e \nu_i(T_e) + n_{e,h} Q_{i,h} v_{h,e}] V. \quad (16)$$

Here ν_{ip} is the average attachment frequency of ions to particles and $\nu_i(T_e)$ the total ionization frequency due to plasma electrons as given in Ref. [51]. ν_{ip} is found by averaging the appropriate OML cross sections of the charged particles over their charge distribution. Even though a dusty plasma behaves as a strongly electronegative plasma, we assume that there is an electropositive region of thickness l in the periphery in which diffusion can be described by the usual ambipolar diffusion coefficient D_a [52].

The energy balance equation is written in a form that the power provided by the radio-frequency field P_{rf} is dissipated in electron collision processes and in ion acceleration in the rf sheaths:

$$P_{\mathrm{rf}} = n_e(\nu_i u_i + \nu_{\mathrm{ex}} u_{\mathrm{ex}}) V + n_i \frac{D_a}{l} A_s e \frac{V_{\mathrm{sh}}}{2}, \quad (17)$$

with $\nu_{\mathrm{ex}}(T_e)$ the average total excitation frequency for plasma electrons as given in Ref. [51]. In a capacitive rf discharge the time averaged rf voltage can be roughly approximated to be 1/2 the maximum sheath voltage V_{sh} or about 1/4 of the peak-to-peak rf voltage.

The quasineutrality condition provides us with a third equation

$$n_i = \overline{Z}(\overline{R_p}) n_p + n_e, \quad (18)$$

where $\overline{Z}(\overline{R_p})$ is the average charge of particles with average radius $\overline{R_p}$ and number density n_p. In this simple model we neglect negative ions, which might be important in an actual Ar:SiH_4 plasma and which might lead to a lower electron density.

The system of equations is closed by two balance equations for the resonant states. For simplicity, we assume that the levels are excited by direct and cascade electron excitation and lost by trapped radiative decay:

$$n_e \nu_{\mathrm{ex}}^{1,2} = n_{1,2} g_{1,2} A_{1,2}. \quad (19)$$

Diffusion as well as excitation or ionization are neglected as loss mechanisms. The excitation frequencies $\nu_{\mathrm{ex}}^{1,2}$ are calculated assuming a Maxwellian electron distribution and using the total (direct+cascade) excitation cross sections given in Ref. [53]. $g_{1,2}$ represents the escape factors for resonance radiations as given by Walsh [54] and Holstein [55]. Since these factors do not account for partial frequency redistribution [56], which is important in the pressure range considered, we use five times lower values for $g_{1,2}$ as suggested by Ferreira and Loureiro [57].

In this system of equations used to compute the plasma properties we approximate the particles as being monodisperse with the particle radius being equal to the average radius of the particle size distribution. This approximation considerably reduces numerical work which would be required to calculate the appropriate averages over the particles size distribution.

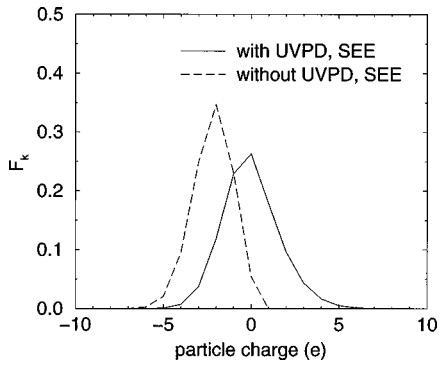

FIG. 1. Particle charge distribution for $T_e = 4.2$ eV, $n_e = 2.45 \times 10^8$ cm^{-3}, and $n_i = 3.5 \times 10^9$ cm^{-3}. The full curve denotes the charge distribution with UVPD and SEE ($Q=1$, $\gamma_i = 0.4$, $\delta = 3.5$), the dashed curve without these processes ($Q=0$, $\gamma_i = 0$).

D. Numerical scheme

We start our simulation with a mono-disperse distribution of primary particles of $R_p = 1$ nm and $n_p = 2 \times 10^{18}$ m^{-3} which corresponds to conditions found by Bouchoule and Boufendi [6,5]. We assume ions, neutral gas molecules and particles to be in thermal equilibrium at a temperature of 300 K. The plasma parameters are calculated and the charge distribution is determined for each section of the particle volume distribution. Integration in time of the sectional model for the particle volume distribution is started. The plasma parameters are updated and the charge distributions and $\alpha(v,v')$ for each section are recalculated whenever the total number of particles has decreased by 20% due to coagulation. This method turns out to be sufficiently accurate and stable to integrate the coagulation process up to 100 s after the onset of coagulation. The total aerosol volume is conserved to better than 10^{-6} relative error. All calculations are performed for the experimental conditions of Bouchoule and Boufendi [6,5]: The diameter of the plasma volume is 13.5 cm and the electrode separation 3.3 cm. The neutral gas pressure is 117 mTorr. The peak-to-peak rf voltage is 600 V, i.e., $V_{\mathrm{sh}} \approx 300$ V. The rf power absorbed by the plasma is 10 W unless noted differently. For the diffusion length l we assume a value of 0.8 cm.

III. RESULTS AND DISCUSSION

A. Impact of UV photodetachment and secondary electron emission on coagulation dynamics and plasma properties

Our initial motivation to study UV photodetachment (UVPD) and secondary electron emission (SEE) was the suspicion that inclusion of these additional effects might lead to more positively charged particles and that attraction of oppositely charged particles might lead to enhanced coagulation in comparison to the too slow coagulation found in the study of Schweigert and Schweigert [22]. Figure 1 shows the charge distributions of particles if UVPD, SEE, and quenching are accounted for ($Q=1$, $\gamma_i = 0.4$, $\delta = 3.5$), and if these effects are turned off ($Q=0$, $\gamma_i = 0$). The plasma conditions

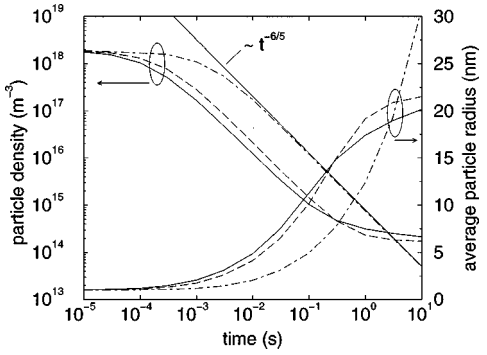

FIG. 2. Particle number density and average radius during coagulation. The full lines denote full UVPD and SEE ($Q=1$, $\gamma_i=0.4$, $\delta=3.5$), the dashed lines reduced UVPD and no SEE ($Q=0.25$, $\gamma_i=0$). The dash-dotted lines show the behavior of a neutral aerosol.

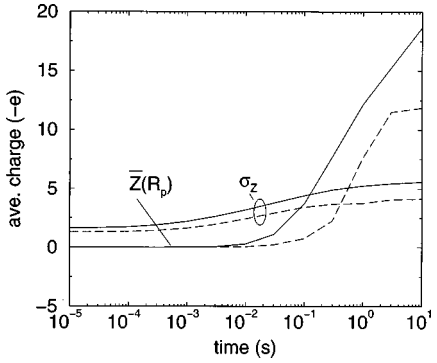

FIG. 3. Average particle charge $\bar{Z}$ and standard deviation σ_Z of the charge distribution for the conditions shown in Fig. 2. Solid lines: with full UVPD and SEE ($Q=1$, $\gamma_i=0.4$, $\delta=3.5$), dashed lines: reduced UVPD and no SEE ($Q=0.25$, $\gamma_i=0$).

correspond to the self-consistent conditions of the former case and are chosen *identical* for both cases. Indeed, the inclusion of UVPD and SEE leads to a considerable fraction of positively charged particles. The case without UVPD and SEE shows a negligible number of positive particles as already observed in Ref. [22]. On the first glance, one might expect that the charge distribution in Fig. 1 which includes UVPD and SEE might yield a faster coagulation rate. However, one has to keep in mind that the plasma properties used in Fig. 1 are *not self-consistent* for the case without UVPD and SEE.

In the following, we now consider *coagulation under self-consistent plasma conditions.* In order to study the influence of UVPD and SEE we compare the particle growth dynamics if these processes are fully taken into account ($Q=1$, $\gamma_i=0.4$, $\delta=3.5$, solid lines), and if they are strongly reduced (SEE turned off, i.e., $\gamma_i=0$ and UVPD reduced by factor $Q=0.25$, dashed lines.) The factor $Q=0$ yields unrealistically high electron temperatures, see below. The effects due to quenching of excited atoms are negligible, as will be shown in the discussion of Fig. 8, and will not be discussed explicitly. For reasons discussed in the context of Fig. 9 we also neglect ionization due to energetic electrons in the ion balance Eq. (16).

Figure 2 shows the particle number density and average radius of the particle distribution function as a function of time during the coagulation process. Surprisingly, the differences in the particle growth dynamics for the cases with full and reduced UVPD and SEE are only minor. While the particle growth is slightly slower with reduced UVPD, the differences in particle volume and particle number density are less than a factor 2 during the entire coagulation process. While the coagulation with UVPD and SEE starts a little faster, the coagulation of particles without UVPD and SEE even leads to slightly larger particles. For comparison, we have also plotted the coagulation dynamics of a neutral aerosol (all particles uncharged, purely thermal coagulation). The coagulation of charged particles is initially considerably faster than the coagulation of neutral particles, as already suspected by Watanabe *et al.* [21]. The coagulation rate of the charged aerosol is about a factor of 10 higher than the coagulation rate of the neutral aerosol. However, after about 0.1–1 s the coagulation of the charged particles starts to slow down since the average particle radius has increased strongly and particles become increasingly negatively charged. After a few seconds the neutral coagulation even takes over and finally yields larger particles after 10 s than in the cases of coagulation in the plasma.

It should be pointed that the temporal behavior of charged-particle coagulation and the neutral coagulation during the main growth phase (10^{-4} – 1 s) is identical in the sense that the total particle density n_p behaves as

$$n_p \propto t^{-6/5}. \tag{20}$$

This temporal behavior can qualitatively be understood by considering the particles as monodisperse. The temporal evolution of n_p is then given by

$$\frac{dn_p}{dt} = -\beta n_p^2, \tag{21}$$

with β from Eq. (13) which involves the correction factor for the collision cross section of charged particles α [Eq. (14)]. Since the particle volume $v \propto 1/n_p$ one finds $\beta \propto n_p^{-1/6}$ and thus

$$\frac{dn_p}{dt} \propto -n_p^{11/6} \quad \Rightarrow \quad n_p \propto t^{-6/5}. \tag{22}$$

The same temporal behavior is also found from more rigorous treatments [48]. The actual rate of coagulation is determined by the value of α. As long as α is constant during the coagulation of charged particles, their temporal coagulation behavior corresponds to that of a neutral aerosol of particles with an effective coagulation cross section $\alpha \pi R_s^2$. This basic behavior has already been observed by Courteille *et al.* [15]. However, we want to point out that it is not possible to conclude from the average particle charge being close to zero that the particle coagulation can be treated as purely neutral. Even if the average particle charge is close to zero the coagulation of particles in the plasma can be considerably faster than that of a neutral aerosol if a sufficient number of positively and negatively charged particles is present. This is exemplified by the plot of the average particle charge and the standard deviation of the charge distribution shown in Fig. 3

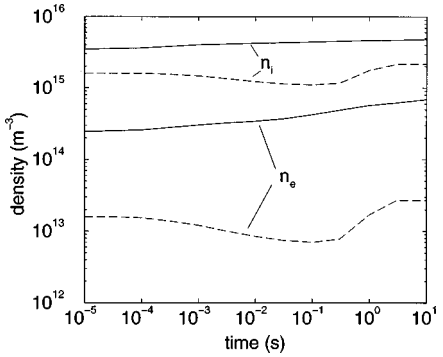

FIG. 4. Electron and ion density during particle coagulation. The designation of the lines and the conditions are the same as in Figs. 2 and 3.

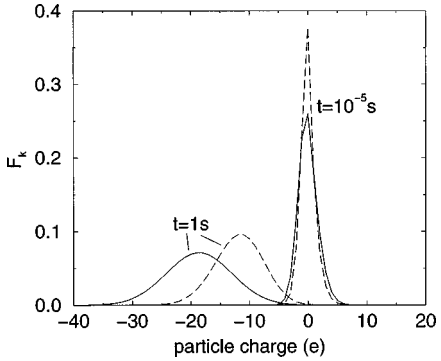

FIG. 6. Particle charge distribution at 10^{-5} and 1 s. The designation of the lines and the conditions are the same as in Figs. 2 and 3.

and the fast coagulation of the charged particles observed in Fig. 2.

As one success of our model we can point out that the particle size observed in our calculations is very close to the size observed in the experiments by Bouchoule and Boufendi [5,6]. The average size of our particles is within about 20% of the experimental results. Our model thus yields a significantly faster coagulation than the model by Schweigert and Schweigert [22] consistent with experiments.

The result that UVPD and SEE should have a considerable influence on the charge distribution (see Fig. 1) but that they seem to have negligible influence on the coagulation dynamics (see Fig. 2) appears slightly paradoxical. The influence of UVPD and SEE seems to disappear in self-consistent calculations. One has to conclude that the plasma properties are different if different charging processes are considered. In other words, there seems to be a significant mutual dependence between plasma properties and particle charging.

In Fig. 4 we show the self-consistent electron and ion densities and the self-consistent electron temperatures in Fig. 5 for the conditions of Fig. 2. Both figures demonstrate that significant differences in these plasma properties result from different efficiencies of the UVPD and SEE. The results for the full UVPD and SEE are generally consistent with experimental results of Boufendi and Bouchoule [6,5]. The ratio of ion to electron density is of the order of 10. For reduced UVPD and no SEE a ratio of about 100 is observed. Also,

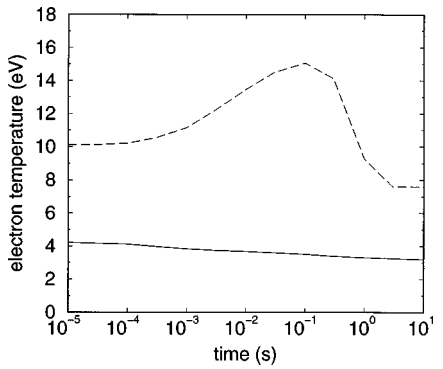

FIG. 5. Electron temperature during particle coagulation. The designation of the lines and the conditions are the same as in Figs. 2 and 3.

while the electron temperatures are quite reasonable for full UVPD and SEE, unrealistically high temperatures are observed for reduced UVPD. Based on investigation of Eq. (16), (17), and (18) we interpret these observations as follows: Due to the fact that the ion acceleration in the sheath is the dominating energy dissipation term in the power balance Eq. (17), the ion density is mostly determined by the rf power absorbed by the plasma. Since we assume the rf power to be constant during coagulation, the positive ion density has to remain almost constant. The quasineutrality implies that the negative charge density—which comprises the free plasma electrons and the negatively charged particles—will also be approximately constant. Thus if UVPD and SEE are reduced, electrons are allowed to remain on the particles longer and the free electron density in the plasma drops. However, since the electrons still have to maintain a sufficient level of ionization, the electron temperature increases. This change in the plasma conditions due to changes in UVPD and SEE in turn also affects the charge distributions of the particles which look much more similar in the two cases with full and reduced UVPD and SEE when self-consistent plasma properties are used, Fig. 6, than in the not self-consistent case, Fig. 1.

From the above results one can conclude that the details of the charging mechanisms have only a minor influence on the coagulation dynamics but a major influence on the plasma properties. Keeping in mind that a model such as the one presented here has to be considered a first step on the way to develop a self-consistent model for a chemically active plasma with particle nucleation and coagulation growth, it is clear that the differences in plasma properties found here are of great importance for the accurate description of the plasma chemistry. Figure 7 shows the dissociation rate of silane for the plasma parameters of Figs. 4 and 5. For the two cases with full and reduced UVPD a difference of more than a factor 3 in the dissociation rate of silane is observed. It is obvious that an accurate description of the plasma chemistry requires accurate knowledge of the details of particle charging.

In Fig. 8 we show the relative importance of the different particle charging mechanisms. The charging frequencies of the particles increase with time due to the increasing particle radius during coagulation. It is obvious that UVPD is the most important effect leading to a positive charge on the particles. The charging frequency of SEE is about a factor of

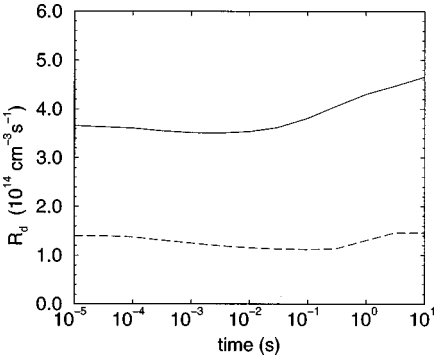

FIG. 7. Dissociation rate of silane for the conditions in Figs. 4 and 5. The partial pressure for silane is assumed to be 4.5 mTorr. The designation of the lines is the same as in Figs. 2 and 3.

5 smaller even though a high value for the secondary electron release at the electrode of $\gamma_i = 0.4$ and a secondary emission coefficient of the particle of $\delta = 3.5$ have been assumed. Quenching of excited atoms is only a minor effect. It should be noted that both electron and ion capture by the particle depend strongly on the particle charge. Thus even if the ion capture frequency of a neutral particle is very small compared to UVPD and SEE, it increases rapidly for negatively charged particles due to the increase of the OLM cross section.

Figure 8 suggests that secondary electrons released at the electrodes only have a small direct impact on the particle charging and particle coagulation dynamics. However, our model shows that these secondary electrons may gain a strong *indirect* influence on the particle charging and coagulation dynamics by modifying the plasma properties. Figure 9 shows the average particle radius and the electron temperature if the main part of the ionization is due to energetic electrons which have been accelerated in the electrode sheaths. The temperature of the plasma electrons becomes rather small in this case. This effect has been observed in pristine argon and helium capacitive rf plasmas by Godyak *et al.* [58]. This low temperature leads to a very narrow charge distribution on the particles. In the late stage of the coagulation process almost all particles carry a single elementary charge, which effectively suppresses coagulation and limits the growth of particles to about 7 nm radius. Even though such small electron temperatures have not been observed in dusty plasma experiments, this result could point to an interesting possibility to limit the coagulation growth of particles by deliberately lowering the electron temperature in the plasma, for instance, by using electron beams or external UV radiation sources to produce additional ionization in the plasma.

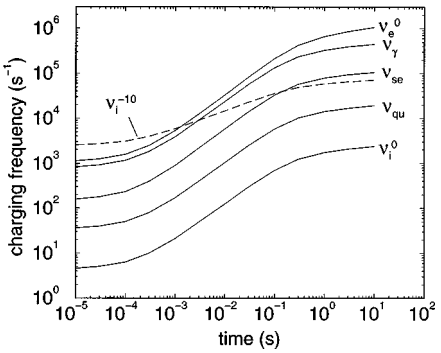

FIG. 8. The charging frequencies for the different charging mechanisms. The conditions are those of full UVPD and SEE from Fig. 2. The superscripts at ν_e and ν_i denote the charging state of the particle.

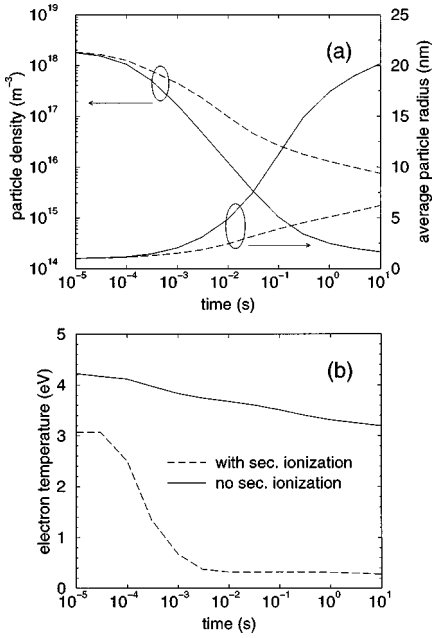

FIG. 9. (a) Average particle density and radius under conditions of dominant ionization due to energetic sheath electrons. (b) Electron temperature for these conditions. Full lines: ionization by energetic electrons is neglected in ion balance, dashed lines: ionization by energetic electrons is taken into account.

B. Critical density for coagulation

In several studies it has been observed that particles grow due to coagulation only if a certain critical density of the primary particles is exceeded. Fridman *et al.* propose that three-particle and higher-order many-particle coagulation events become important when the critical density is approached [16]. This assumption, however, seems to be rather unlikely. For instance, for the initial density of 2×10^{12} cm^{-3} coagulation is clearly observed. However, the three-particle coagulation frequency is by at least one order of magnitude smaller than the two-particle coagulation frequency. Higher order collisions are even less frequent. Also, the temporal behavior of the particle density during the main coagulation phase is close to the $t^{-6/5}$ for neutral coagulation which can be derived assuming only two-particle collisions.

In Fig. 10 we study the influence of the initial density on the coagulation process. Also shown is the positive ion density, which corresponds to these conditions. It can be observed that coagulation is slowed down compared to neutral coagulation ($t^{-6/5}$ behavior) if the particle density has decreased so far that it equals the positive ion density. This means that the average particle charge is about one elementary charge so that particle charging becomes a notable factor to suppress coagulation. This interpretation is also evidenced by Fig. 11 in which the coagulation for constant initial density is studied for different rf powers, i.e., different positive

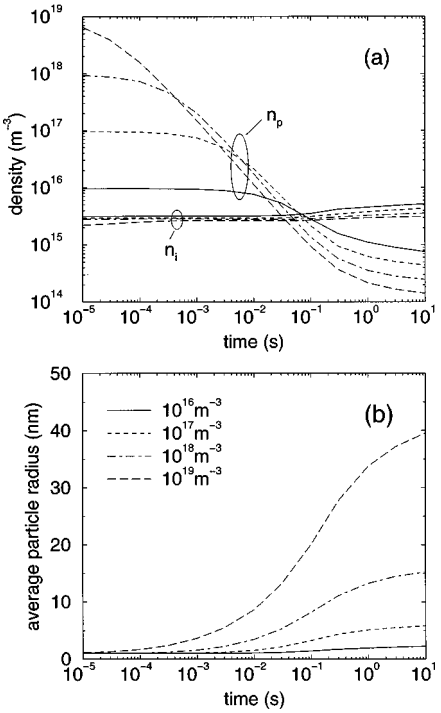

FIG. 10. Temporal evolution of (a) the particle density and ion density and (b) the particle radius for various values of the initial particle density.

ion densities. Again it can be observed that the coagulation is notably slowed down once the particle density reaches the value of the positive ion density.

These results suggest that as a rule of thumb *the positive ion density in the plasma can be considered the critical density for coagulation*. If the initial particle density does not exceed the positive ion density, most particles will be negatively charged and particles will be prevented from coagulating. In this case particles are likely to grow due to surface deposition. The initial particle density depends on the particular plasma chemistry and the discharge parameters. Our model is not capable of predicting initial densities since neither nucleation of initial particles nor loss mechanisms are currently considered. However, in principle the initial particle density can be determined from the balance of the nucleation rate and the loss rate of particles to the discharge walls.

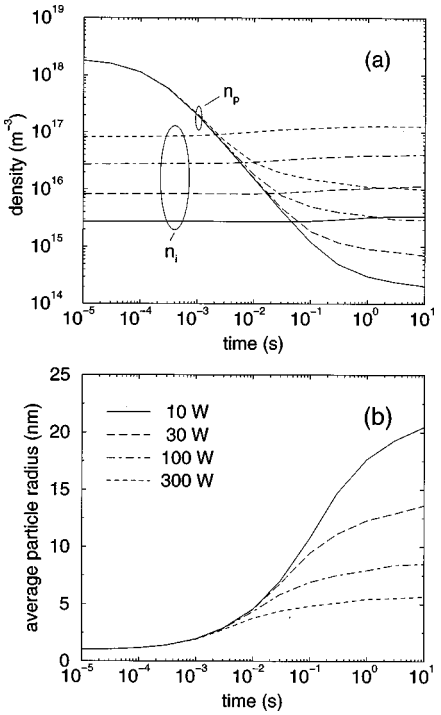

FIG. 11. Temporal evolution of (a) the particle density and the ion density and (b) the particle radius for different rf powers.

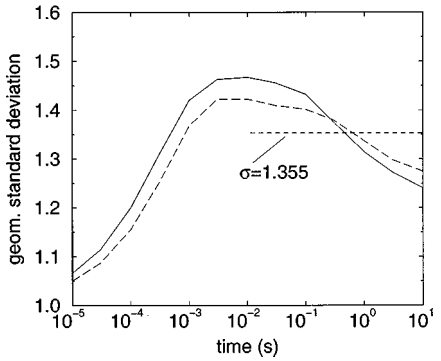

FIG. 12. Temporal evolution of the geometric standard deviations σ of the log-normal distributions fitted to the particle size distribution for the conditions in Fig. 2.

C. Details of the particle size distribution

In the literature about coagulation of neutral aerosols the particle size distribution is frequently approximated by a log-normal distribution function

$$n(R_p) \propto \frac{A}{\ln \sigma} \exp\left(- \frac{\ln^2(R_p/R_g)}{2 \ln^2 \sigma} \right), \tag{23}$$

with R_g the geometric mean radius and σ the geometric standard deviation. Our results show that also in the case of particle coagulation in low pressure plasmas the particle size distribution can well be approximated by a log-normal distribution. Interestingly, it is known that for neutral aerosols the geometric standard deviation σ approaches a universal value of 1.355 regardless of the σ of the initial distribution [48]. In Fig. 12 we show σ values obtained for the particle distribution functions for our conditions. The log-normal distribution of charged particles at the end of the coagulation process has a smaller σ than the asymptotic value 1.355 for neutral aerosols. The reason is probably that particles at the large size end of the distribution are already all mostly negatively charged so that coagulation is suppressed. Particles at the small size end of the distribution still have a charge distribution with a certain fraction of neutral and positive particles which are still able to coagulate with other particles. Thus the coagulation at the large size end is slowed down while the coagulation loss of small particles depletes the small size end of the distribution which leads to a contraction of the distribution compared to a neutral aerosol.

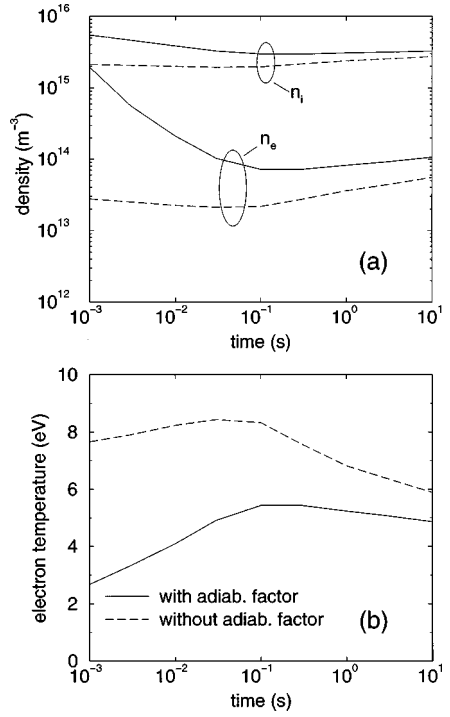

FIG. 13. (a) Electron and ion densities and (b) electron temperatures with (full lines) and without adiabatic factor (dashed lines).

D. Impact of the ''adiabatic factor''

It has to be pointed out that the temporal behavior of electron and ion densities in the plasma as shown in Fig. 4 does not correspond to experimental observations. For instance, Stoffels *et al.* [59] report a relatively slow drop of the electron density from the value in the quasineutral plasma to a value about a factor 10 less over a time of about 1 s. Bouchoule and Boufendi report an increase of the line emission of argon lines over a time of a few seconds during coagulation which suggests that the electron temperature increases slowly with the same time scale. Our calculations on the other hand show that the plasma conditions adjust to the presence of particles almost immediately. This is not a consequence of our assumption of a steady state charge distribution. In particular, the attachment frequency of electrons to particles is of the order of 10^6 s^{-1}. Thus one would have to expect that electron density and temperature show variations on a time scale of some microseconds. The experimental results of Stoffels *et al.* and Bouchoule and Boufendi seem to suggest that the frequency of electron attachment to the particles is actually much smaller than the one given by Eq. (1). This was also pointed out by Fridman *et al.* [16] who proposed an ''adiabatic factor'' which is a size-dependent sticking factor for the electrons to nanometer-sized particles. The ''adiabatic factor'' describes that the kinetic energy of the electron has to be transferred to vibrational excitation of the particle via polarization [16].

We have studied the influence of the adiabatic factor on the plasma properties in our simulation. The influence on the coagulation dynamics of the particles (not shown here) is only minor, since the coagulation is not significantly affected by the details of the particle charging mechanisms. Figure 13 shows the temporal evolution of the plasma properties with and without adiabatic factor used in Eq. (1). Both, the behavior of the electron density and the electron temperature show a relatively slow variation on a time scale of 0.1 s if the adiabatic factor is used. The temporal evolution of the plasma properties is thus in much better agreement to experiments if the adiabatic factor is used.

The above results seem to suggest that the adiabatic factor proposed by Fridman *et al.* realistically describes the electron attachment to particles. However, the use of this factor seems to be in contradiction to recent results of a quantum-mechanical treatment of the electron-attachment to particles by Perrin [40]. The author finds that for hydrogenated silicon particles consisting of only 1000 atoms (about 2 nm diameter) the attachment probability for electrons with energies below 10 eV is almost one. Due to these controversial results and based on the fact that the adiabatic factor plays only a minor role for the coagulation dynamics we have not generally used this factor in this study.

IV. SUMMARY AND CONCLUSION

In this section we summarize our main results and comment on their importance and possible implications

(1) As a rule of thumb, *the positive ion density in the plasma constitutes the critical density for the coagulation process*. The initial particle density, which is determined by the balance of nucleation and particle losses, has to considerably exceed the positive ion density in the plasma so that coagulation can occur.

This result could explain why particles due to gas phase nucleation and coagulation have been observed in PECVD plasmas which typically operate at gas pressure of about 100 mTorr and low plasma density (10^9-10^{10} cm^{-3}) and not in high density etching plasmas which operate at about ten times lower gas pressure and 100–1000 times higher plasma density. However, this result cannot be interpreted to the extent that coagulation in PECVD plasmas can be avoided by increasing the plasma density since this typically also increases the rate of plasma chemical reactions and thus the nucleation rate. As a consequence of a higher plasma density also a larger primary particle density has to be expected.

(2) As long as the particle density is higher than the positive ion density, coagulation of particles in a plasma follows the same time dependence as neutral coagulation ($n_p \propto t^{-6/5}$). In this sense charged particle coagulation can be considered as neutral coagulation of particles with an effective coagulation cross section $\alpha \pi R_s^2$ which depends on the particle charge distribution. The details of the charging mechanism do not have a considerable influence on the coagulation dynamics.

(3) The details of the charging mechanisms strongly affect results for the self-consistent plasma properties. Basically, a decrease of detachment of electrons allows electrons to stay on the particles longer and leads to a smaller plasma electron density. Since ionization has to remain approximately constant this is balanced by a higher electron temperature.

It should be mentioned that these changes in the plasma properties would result in significantly different conditions for the chemistry of chemically active plasmas. It should also be stressed that our discussion of UVPD and SEE is purely based on speculation about the actual values of quantum yields and secondary emission coefficients. These basic

properties of nanometer particles are widely unknown. However, they are obviously of great importance for accurate plasma modeling in nanometer-particle containing plasmas. We conclude that there is great need for experimental and theoretical studies to determine these basic properties of nanoparticles.

(4) We have shown that energetic sheath electrons can gain a large, indirect influence on the coagulation dynamics. If energetic sheath electrons take over the ionization, the electron temperature of the plasma electrons decreases strongly. As a consequence the charge distribution of particles becomes very narrow with almost all particles being singly negatively charged in the last stage of coagulation. This typically stops coagulation of particles at a smaller size than in cases when the plasma electron temperature remains high.

This observation could actually point a way to controlling the final size of particles during the coagulation process. For instance, one could imagine using electron beams or external UV radiation to produce additional ionization in the plasma and to reduce the electron temperature of the plasma electrons.

(5) Our calculations show that the ''adiabatic factor'' [16] yields more realistic plasma properties than the assumption of an electron sticking factor of unity. However, controversial statements about the probability of electron attachment to nanometer particles are found in the literature. It seems that there is a definite need for experimental studies of this topic.

This study is only a first step on the way to self-consistent modeling of gas phase growth of particles in low pressure plasmas. A more complete approach will require the modeling of the particle nucleation, including the effect of non-Maxwellian electron distribution functions, as well as inclusion of particle losses in spatially inhomogeneous plasmas. Work on this topic is in progress and will be reported in future publications.

ACKNOWLEDGMENT

This work was supported by the National Science Foundation under Grant No. ECS-9731568.

[1] R. M. Roth, K. G. Spears, G. D. Stein, and G. Wong, Appl. Phys. Lett. **46**, 253 (1985).
[2] G. S. Selwyn, J. Singh, and R. S. Bennet, J. Vac. Sci. Technol. A **7**, 2758 (1989).
[3] G. M. Jellum and D. B. Graves, J. Appl. Phys. **67**, 6490 (1990).
[4] J. S. Logan and J. J. McGill, J. Vac. Sci. Technol. A **10**, 1875 (1992).
[5] A. Bouchoule and L. Boufendi, Plasma Sources Sci. Technol. **2**, 204 (1993).
[6] L. Boufendi and A. Bouchoule, Plasma Sources Sci. Technol. **3**, 263 (1994).
[7] M. P. Garrity, T. W. Peterson, and J. F. O'Hanlon, J. Vac. Sci. Technol. A **14**, 550 (1996).
[8] F. Vivet and A. Bouchoule, in *XIII International Conference on Phenomena in Ionized Gases, ICPIC*, Toulouse, July, 1997, edited by M. C. Bordage and A. Gleizes (CPAT, Toulouse, France, 1997), Vol. 1.
[9] F. Vivet, A. Bouchoule, and L. Boufendi, J. Appl. Phys. **83**, 7474 (1998).
[10] P. Roca i Cabarrocas, P. Gay, and A. Hadjadj, J. Vac. Sci. Technol. A **15**, 655 (1996).
[11] D. M. Tanenbaum, A. L. Laracuente, and A. Gallagher, Appl. Phys. Lett. **68**, 1705 (1996).
[12] P. Roca i Cabarrocas, P. St'ahel, and S. Hamma, in *Proceedings of the Second World Conference on Photovoltaic Solar Energy Conversion, Vienna, 1998*, edited by J. Schmid, H. A. Ossenbrink, P. Helm, H. Ehmann, and E. D. Dunlop, European Commission Joint Research Center Report No. EUR 18656 EN (1998), p. 355.
[13] P. R. i Cabarrocas, S. Hamma, S. N. Sharma, J. Costa, and E. Bertran, J. Non-Cryst. Solids **227**, 871 (1998).
[14] Y. Watanabe, M. Shiratani, T. Fukuzawa, H. Kawasaki, Y. Ueda, S. Singh, and H. Ohkura, J. Vac. Sci. Technol. A **14**, 995 (1996).
[15] C. Courteille, C. Hollenstein, J.-L. Dorier, P. Gay, W. Schwarzenbach, A. A. Howling, E. Bertran, G. Viera, R. Martins, and A. Mararico, J. Appl. Phys. **80**, 2069 (1996).
[16] A. A. Fridman, L. Boufendi, T. Hbid, B. V. Potapkin, and A. Bouchoule, J. Appl. Phys. **79**, 1303 (1996).
[17] J. Perrin, C. Böhm, R. Etemadi, and A. Lloret, Plasma Sources Sci. Technol. **3**, 253 (1994).
[18] J. Goree, Plasma Sources Sci. Technol. **3**, 400 (1994).
[19] T. Matsoukas, M. Russel, and M. Smith, J. Vac. Sci. Technol. A **14**, 624 (1996).
[20] T. Matsoukas, J. Colloid Interface Sci. **187**, 474 (1997).
[21] Y. Watanabe, M. Shiratani, H. Kawasaki, S. Singh, T. Fukuzawa, Y. Ueda, and H. Ohkura, J. Vac. Sci. Technol. A **14**, 540 (1996).
[22] V. A. Schweigert and I. V. Schweigert, J. Phys. D **29**, 655 (1996).
[23] K.-S. Kim and M. Ikegawa, Plasma Sources Sci. Technol. **5**, 311 (1996).
[24] J. E. Allen, Phys. Scr. **45**, 497 (1992).
[25] Y. Liu, Q.-L. Zhang, F. K. Tittel, R. F. Curl, and R. E. Smalley, J. Chem. Phys. **85**, 7434 (1986).
[26] O. Chesnovsky, S. H. Yang, C. L. Pettiette, M. J. Craycraft, Y. Liu, and R. E. Smalley, Chem. Phys. Lett. **138**, 119 (1987).
[27] K. Fuke, K. Tsukamoto, F. Misaizu, and M. Sanekata, J. Chem. Phys. **99**, 7807 (1993).
[28] C. C. Arnold, T. N. Kitsopoulos, and D. M. Neumark, J. Chem. Phys. **99**, 766 (1993).
[29] C. Xu, T. R. Taylor, G. R. Burton, and D. M. Neumark, J. Chem. Phys. **108**, 1395 (1998).
[30] A. Schmidt-Ott, P. Schurtenberger, and H. C. Siegmann, Phys. Rev. Lett. **45**, 1284 (1980).
[31] H. Burtscher, L. Scherrer, H. C. Siegmann, A. Schmidt-Ott, and B. Federer, J. Appl. Phys. **53**, 3787 (1982).
[32] H. Burtscher, A. Schmidt-Ott, and H. Siegmann, Z. Phys. B **56**, 197 (1984).

[33] T. Jung, H. Burtscher, and A. Schmidt-Ott, J. Aerosol Sci. **4**, 485 (1988).
[34] U. Müller, M. Ammann, H. Burtscher, and A. Schmidt-Ott, Phys. Rev. B **44**, 8284 (1991).
[35] B. Schleicher, H. Burtscher, and H. C. Siegmann, Appl. Phys. Lett. **63**, 1191 (1993).
[36] U. Müller, H. Burtscher, and A. Schmidt-Ott, Phys. Rev. B **38**, 7814 (1988).
[37] D. M. Wood, Phys. Rev. Lett. **46**, 749 (1981).
[38] T. Holstein, Phys. Rev. **72**, 1212 (1947).
[39] C. Böhm and J. Perrin, Rev. Sci. Instrum. **64**, 31 (1993).
[40] J. Perrin and C. Hollenstein, in *Dusty Plasmas*, edited by A. Bouchoule (Wiley, New York, in press), Chap. II.
[41] C. Seigneur, A. B. Hudischewskyi, J. H. Seinfeld, K. T. Withby, E. R. Withby, J. R. Brock, and H. M. Barnes, Aerosol. Sci. Technol. **5**, 205 (1986).
[42] A. Oron, J. H. Seinfeld, and K. Okuyama, J. Colloid Interface Sci. **133**, 57 (1989).
[43] A. Oron and J. H. Seinfeld, J. Colloid Interface Sci. **133**, 66 (1989).
[44] A. Oron and J. H. Seinfeld, J. Colloid Interface Sci. **133**, 880 (1989).
[45] Y. Xiong, S. E. Pratsinis, and S. V. R. Mastrangelo, J. Colloid Interface Sci. **153**, 106 (1992).
[46] S. Vemury, C. Janzen, and S. E. Pratsinis, J. Aerosol Sci. **28**, 599 (1997).
[47] H. Muller, Kolloidbeihefte **27**, 223 (1928).
[48] K. W. Lee, H. Chen, and J. A. Gieske, Aerosol. Sci. Technol. **3**, 53 (1984).
[49] F. Gelbard, Y. Tambour, and J. H. Seinfeld, J. Colloid Interface Sci. **76**, 541 (1980).
[50] J. D. Landgrebe and S. E. Pratsinis, J. Colloid Interface Sci. **139**, 63 (1990).
[51] U. Kortshagen, N. D. Gibson, and J. E. Lawler, J. Phys. D **29**, 1224 (1996).
[52] A. J. Lichtenberg, I. G. Kouznetsov, Y. T. Lee, M. A. Lieberman, I. D. Kaganovich, and L. D. Tsendin, Plasma Sources Sci. Technol. **6**, 437 (1997).
[53] C. M. Ferreira and J. Loureiro, J. Phys. D **16**, 1611 (1983).
[54] P. J. Walsh, Phys. Rev. **116**, 511 (1959).
[55] T. Holstein, Phys. Rev. **83**, 1159 (1951).
[56] J. E. Lawler and J. J. Curry, in *Electron Kinetics and Applications of Glow Discharges*, Vol. 367 of *NATO Advanced Studies Institute, Series B: Physics*, edited by U. Kortshagen and L. D. Tsendin (Plenum, New York, 1998), p. 471.
[57] C. M. Ferreira, J. Loureiro, and A. Ricard, J. Appl. Phys. **57**, 82 (1985).
[58] V. A. Godyak, R. B. Piejak, and B. M. Alexandrovich, Phys. Rev. Lett. **68**, 40 (1992).
[59] E. Stoffels, W. W. Stoffels, G. M. W. Kroesen, and F. J. de Hoog, J. Vac. Sci. Technol. A **14**, 556 (1996).